ABSTRACT
A variation of the Chamberlin Trimetric map projection is presented, termed the Matrix Trimetric projection. The Matrix Trimetric projection amounts to a linear transformation of the squares of the distances from a given point to three control points. It is significantly more efficient to calculate than the Chamberlin projection, and allows for an inverse projection in the spherical approximation which requires numerical iteration of only one parameter. Comparisons between the two projections are made using a representative list of control points. The Chamberlin projection outperforms the Matrix projection on measures of angle deformation and scale deformation, but the reverse is true for a measure of distance deformation. In general the difference between the projections is small.

A variation on the Chamberlin Trimetric map projection

Author

ARTICLE HISTORY
Compiled December 8, 2020

1. Introduction

A map projection is a projection from a sphere or an ellipsoid – such as one being used to model the surface of the Earth – to the plane. Map projections that preserve angles are called conformal; ones that preserve the relative area of shapes may be termed authalic, equal-area, equiareal or equivalent. No map projection preserves distances between all points, but a map projection that preserves distances along certain geodesics may be termed equidistant. All map projections introduce some form of distortion: no map projection may be both conformal and authalic.(Snyder, 1987) A compromise map projection is one that is neither conformal, authalic, or equidistant, but seeks to balance different kinds of distortion.

The Chamberlin Trimetric projection is a compromise map projection that achieves a balance between distortions in area, angle, and distance. It is named for Wellman Chamberlin, a chief cartographer for the National Geographic Society, which has published wall and atlas maps using this projection. The Chamberlin projection is appropriate for mapping whole continents and large portions of continents. The Chamberlin projection has a simple geometric construction, shown in Figure 1. Three control points on the globe are specified, and a triangle in the plane is constructed having the same distances between its vertices as the true distances between the points on the globe. True distances from those control points to a given point on the globe are measured, and arcs are drawn at those distances from their respective points in the plane. The arcs form a small triangle: a point in that triangle is chosen as the projection of the original point.(Christensen, 1992) Originally, in the 1950s when manual plotters were used, the exact definition of this point was not important, but Christensen (1992) and most modern implementations (e.g. PROJ contributors (2019)) use the centroid of the small triangle. Thus, the Chamberlin projection is a form of triangulation: it is also a cousin of the two-point equidistant projection.(Snyder & Voxland, 1989)

The geometric nature of this construction result in a somewhat involved algorithmic form for the Chamberlin Trimetric projection. As commented on in Christensen (1992), the algorithmic form has special cases to handle when the given point lies at a control point, or on an edge of the triangle with vertices at the control points. This also makes analysis of the projection somewhat more difficult, although numerical analysis of the distortion can be performed.

This text presents a new map projection called the Matrix Trimetric projection. A geometric construction related to the Chamberlin Trimetric results in a map projection that is very similar but has a simpler analytical formula. The formula is simply the

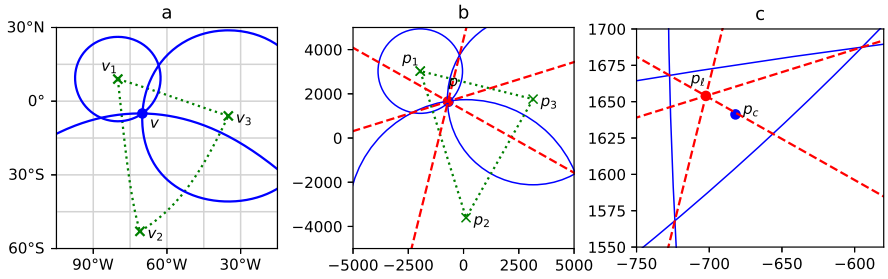

Figure 1. Construction of the Chamberlin and Matrix Trimetric projections. Plot 1a is in equirectangular projection. Plot 1b is the projection to the plane. Plot 1c is the same as plot 1b, zoomed in to the small triangle created by the three circles. $\mathbf{p}_c$ is the point projected by the Chamberlin projection and $\mathbf{p}_m$ is the point projected by the Matrix Trimetric projection. Green solid lines indicate the control triangles, the circles are blue dots, and the perpendiculars are red dashes.

product of a matrix with a vector whose values are the square of the distances from the given point to the control points, thus the name. The differences between the Matrix Trimetric and Chamberlin projections are difficult to notice with the naked eye. The Matrix Trimetric projection introduces slightly more distortion in scale and angle, but less in a distance measurement that will be defined later.

2. Definitions and assumptions

We use the spherical approximation to the Earth. For this text, we assume a sphere with a radius of 6,371 km. The Chamberlin and Matrix projections are compromise projections, and do not perfectly preserve angle, area, or distance. For most practical ellipsoids, distortions due to the spherical approximation are negligible compared to distortions due to the projection itself. If desired, one can use an ellipsoid for distance calculations: the form of the forward formula does not change, but the inverse formula is no longer valid. One can also use an auxiliary latitude: see Snyder (1987) for details.

$\mathbf{v}$ and subscripted versions shall denote points on the sphere, and $\mathbf{p} = [x,\ y]$ and subscripted versions shall denote points in the Euclidean plane. Representing the points on the sphere as a unit vector allows one to apply the tools of linear algebra. Refer to a basic text on linear algebra, such as Strang (1980), if needed. Let latitude be φ and longitude be λ, then latitude and longitude can be converted to a unit vector as so:

$$\mathbf{v} = \begin{bmatrix} x \\ y \\ z \end{bmatrix} = \begin{bmatrix} \cos(\varphi)\cos(\lambda) \\ \cos(\varphi)\sin(\lambda) \\ \sin(\varphi) \end{bmatrix}.$$

The conversion from a unit vector to latitude and longitude is:

$$\begin{aligned} \varphi &= \arctan\left(z, \sqrt{y^2 + x^2}\right) \\ \lambda &= \arctan\left(y, x\right) \end{aligned} \tag{1}$$

where the 2-variable form of arctan is used, commonly called `arctan2` or `atan2` in numeric libraries.

The spherical distance between two unit vectors is

$$d(\mathbf{v}_i, \mathbf{v}_j) = R \arccos(\mathbf{v}_i \cdot \mathbf{v}_j) = \arctan(\|\mathbf{v}_i \times \mathbf{v}_j\|, \mathbf{v}_i \cdot \mathbf{v}_j)$$

where R is the radius of the Earth. The latter form, using the 2-variable form of arctan, is the most numerically stable. Euclidean distances are found using the usual Euclidean norm: $\|\mathbf{p}_a - \mathbf{p}_b\|$.

Let $\mathbf{v}_1$, $\mathbf{v}_2$, $\mathbf{v}_3$ be control points on the sphere: also let $\mathbf{V}$ be the matrix having $\mathbf{v}_i$ as its ith column. Let $\mathbf{p}_1 = [x_1,\ y_1]$ etc. be the control points on the plane. The triangles with vertices at $\mathbf{v}_i$ or $\mathbf{p}_i$ are called the control triangles (spherical or planar control triangle, respectively, if the distinction is important). For this paper, the control triangle is not allowed to have very small or zero area, e.g. the control points lie on a line or are close together. We also exclude the case where all three points of the spherical control triangle lie on the same great circle. None of these cases are typical use cases for the Chamberlin projection. Note that the planar control triangle is **not** the image of the spherical control triangle under either projection. The image of the spherical control triangle is slightly larger, and does not have straight edges.

$\mathbf{p}_i$ must be arranged such that $d(\mathbf{v}_i, \mathbf{v}_j) = \|\mathbf{p}_i - \mathbf{p}_j\|$ for all i and j in $\{1, 2, 3\}$: the spherical length of the edges of the spherical control triangle are equal to the Euclidean lengths of the planar control triangles. Without loss of generality, also assume that $\|\mathbf{p}_i\|$ is the same for all i, such that the center of the circumcircle of the control triangle lies at the origin. This just removes a translation in the plane in order to simplify the formulas; false northing and easting can be added later. Given $\mathbf{v}_i$, $\mathbf{p}_i$ can be constructed as follows. Let i, j, k be a cyclic permutation of $\{1, 2, 3\}$, and let $s_k = d(\mathbf{v}_i, \mathbf{v}_j)$. The circumradius of the Euclidean triangle with sides of length s_k is

$$C = \frac{\prod_i s_i}{\sqrt{\sum_i s_i^2 s_{i+1}^2 - s_i^4}}. \tag{2}$$

From the (Euclidean) law of cosines, the interior angle ϕ_i at each vertex is

$$\phi_i = \arccos\left(\frac{s_k^2 + s_j^2 - s_i^2}{2 s_k s_j}\right). \tag{3}$$

Let $\mathbf{P}$ be the matrix whose ith column is the vector $\mathbf{p}_i$. Then a set of points satisfying the requirements are given as so:

$$\mathbf{P} = \begin{bmatrix} C\cos(2\phi_1) & C\cos(2\phi_0) & C \\ C\sin(2\phi_1) & -C\sin(2\phi_0) & 0 \end{bmatrix}. \tag{4}$$

These points can be rotated about the origin as desired.

To measure distortion of area and angle, we use the area scale factor s and maximum angular deformation ω as defined in equations 12–15, 27, and 28 in section 4 of Snyder (1987). Derivatives are estimated numerically using second-order central differences on a 1-degree grid via the `gradient` function in Numpy.(Harris et al., 2020) There is no standard measurement of distance distortion for map projections, as most map projections fix one or no points. For the projections in this text, it makes sense to measure distances from the control points. Let r_i be the distance from $\mathbf{v}_i$ to $\mathbf{v}$ on the sphere, as earlier, and let ℓ_i be the distance from $\mathbf{p}_i$ to $\mathbf{p}$ in the plane. The measure,

denoted D, is the sum of differences in the distances measured on projected and unprojected distances:

$$D = \sum_i |r_i - \ell_i| \,. \tag{5}$$

3. Forward projection

Let $r_i = d(\mathbf{v}_i, \mathbf{v})$ be the spherical distance from $\mathbf{v}_i$ to $\mathbf{v}$, but also the radius of a circle on the sphere surface such that $\mathbf{v}_i$ is the center and $\mathbf{v}$ lies on the circle's boundary. The Chamberlin projection draws a circle of radius r_i around each point $\mathbf{p}_i$, forming a small triangle with circular arcs for edges, and chooses a point $\mathbf{p}_c$ as the centroid of that small triangle. Of course, each pair of circles intersects in at most two places, so the implementation must take care to choose the point of intersection that lies on the small triangle and not the other.

One can make two observations on this configuration of circles in the plane. One is that the two points of intersection of each pair of circles are symmetric about the triangle edge between the two control points. The other is that, if one draws a line through the two points of intersection of each pair of circles, that line is perpendicular to the triangle edge. These are the dashed red lines in Figure 1. Once the lines are drawn for each pair of circles, the three lines appear to meet at the same point. This can be proven with a simple triangle theorem sometimes attributed to Carnot.(Posamentier & Salkind, 2012)(Wohlgemuth, 2010) Although that point is not necessarily within the small triangle, it is for most points within the control triangle.

The equations of each perpendicular line, taken together, create a linear system. It is an overdetermined system of 3 equations in 2 variables, but since all 3 lines meet at the same point, it has a solution. Ultimately this system can be solved for $\mathbf{p}_m$ to define a forward map projection as follows.

$$\mathbf{p}_m = \mathbf{M} \begin{bmatrix} r_1^2 & r_2^2 & r_3^2 \end{bmatrix}^\top , \tag{6}$$

$$\mathbf{M} = \frac{1}{2T} \begin{bmatrix} y_3 - y_2 & y_1 - y_3 & y_2 - y_1 \\ x_2 - x_3 & x_3 - x_1 & x_1 - x_2 \end{bmatrix} = \frac{1}{2T} \begin{bmatrix} 0 & -1 \\ 1 & 0 \end{bmatrix} \mathbf{P} \begin{bmatrix} 0 & -1 & 1 \\ 1 & 0 & -1 \\ -1 & 1 & 0 \end{bmatrix}, \tag{7}$$

$$T = \begin{vmatrix} x_1 & x_2 & x_3 \\ y_1 & y_2 & y_3 \\ 1 & 1 & 1 \end{vmatrix} . \tag{8}$$

T is equal to twice the area of the Euclidean control triangle.

The matrix $\mathbf{M}$ has a (right) nullspace spanned by the vector $[1, 1, 1]$. This implies the Matrix Trimetric projection is not one-to-one for all possible values of r_i: for example, for any values of r_i such that $r_1 = r_2 = r_3$, then $\mathbf{p}_m = [0, 0]$. Both the Chamberlin and Matrix Trimetric projections project the entire sphere to a bounded portion of the plane. This can be termed the boundary of the projection. There is a region of overlap that is mapped into the same area but in reverse orientation. That

region includes the antipodes of the control points. In real applications, the overlap region can be excluded.

4. Inverse projection

Given $\mathbf{p}_m$, start to invert the projection as so:

$$\begin{bmatrix} k_1 & k_2 & k_3 \end{bmatrix}^\top = \mathbf{M}^+ \mathbf{p}_m, \tag{9}$$

$$\mathbf{M}^+ = \frac{2}{3} \begin{bmatrix} 2x_1 - x_2 - x_3 & 2y_1 - y_2 - y_3 \\ -x_1 + 2x_2 - x_3 & -y_1 + 2y_2 - y_3 \\ -x_1 - x_2 + 2x_3 & -y_1 - y_2 + 2y_3 \end{bmatrix} = \frac{2}{3} \begin{bmatrix} -2 & 1 & 1 \\ 1 & -2 & 1 \\ 1 & 1 & -2 \end{bmatrix} \mathbf{P}^\top \tag{10}$$

$k_i = r_i^2 - h$ for some value h. This is a general solution to inverting Equation 6, thus the free parameter h. $\mathbf{M}^+$ is the pseudoinverse of $\mathbf{M}$ and vice versa. Because $\mathbf{M}^+$ has a left nullspace spanned by the vector $[1, 1, 1]$, it follows that $\sum_i k_i = 0$, which can be used to skip some steps in calculating of k_i.

Plugging Equation 6 into Equation 9 reveals that $h = \frac{1}{3} \sum_i r_i^2$. Unfortunately, if one attempts to solve for r_i given k_i, they find another general solution with one free parameter, putting them right back where they started. It turns out that information about the sphere needs to be introduced to determine r_i and $\mathbf{v}$.

For the following, let r_i have units of radians of arc on the surface of the sphere, i.e. $R = 1$. This does not affect the result or require unit conversion in implementation, it just makes the derivation simpler. The circle of points $\mathbf{v}$ at distance r_0 from a point $\mathbf{v}_0$ is simply the circle where a plane intersects the sphere. This plane may be specified as $\mathbf{v}_0 \cdot \mathbf{v} = \cos(r_0)$. Replacing $\mathbf{v}_0$ with $\mathbf{v}_i$ and r_0 with r_i for each i gives a linear system. Thus,

$$\mathbf{v} = \mathbf{V}^{-1} \begin{bmatrix} \cos(r_1) \\ \cos(r_2) \\ \cos(r_3) \end{bmatrix}. \tag{11}$$

For the point to lie on the unit sphere, $\|\mathbf{v}\| = 1$. Let $\mathbf{c}$ be a vector with ith component $\cos(r_i)$. Then, $\mathbf{c}^\top \left(\mathbf{V}^\top \mathbf{V}\right)^{-1} \mathbf{c} = 1$. Make the substitution

$$r_i = \sqrt{k_i + h}. \tag{12}$$

We now have an equation with one unknown, h.

Some obvious bounds can be placed on h. In units of radians, $0 \leq r_i \leq \pi$. Since this must hold for every r_i, it follows that

$$-\min_i k_i \leq h \leq \pi^2 - \max_i k_i. \tag{13}$$

Within these bounds, there may be at most two solutions for h. The solution with smaller h is the desired one, and the one with larger h corresponds to the overlap region.

Let

$$f(h) = \mathbf{c}^\top \mathbf{A}\mathbf{c} - 1. \tag{14}$$

where $\mathbf{A} = \left(\mathbf{V}^\top \mathbf{V}\right)^{-1}$ is symmetric and positive semi-definite. The derivative of $f(h)$ is

$$f'(h) = -\mathbf{c}^\top \mathbf{A}\mathbf{b} \tag{15}$$

where $\mathbf{b}$ is a vector with ith component $\operatorname{sinc}\left(\sqrt{k_i + h}\right)$. Note that $f'(h)$ and $f(h)$ share many of the same terms, a fact that can be exploited to make the calculation more efficient.

The lower solution for $\mathbf{p}_m = [0, 0]$ is a global minimum for h, and can be calculated analytically as so:

$$h_0 = \arccos\left(\frac{1}{\sqrt{\sum \mathbf{A}}}\right)^2 \tag{16}$$

where $\sum \mathbf{A}$ denotes the sum of all entries in the matrix $\mathbf{A}$.

Given all the preceding, Newton's method can be applied to solve for h. A suitable initial condition is

$$h_{\min} = \max\left(h_0, -\min_i k_i\right), \tag{17}$$

which appears to always result in convergence to the lower root of $f(h)$. One could use $\frac{1}{3}\sum_i l_i^2$, where $l_i = |\mathbf{p}_m - \mathbf{p}_i|$ approximates r_i fairly well, but for some $\mathbf{p}_m$ near the boundary of the projection the iteration converges to the higher root.

A good approximation is achieved for points inside the control triangle within only a few iterations. Convergence is somewhat slower further away from the control triangle, and is worst at the boundary of the projection. This is expected: at the boundary, the lower solution and upper solution are the same and $f(h) = f'(h) = 0$ so Newton's method converges at a merely linear rate.(Burden & Faires, 2006)

5. Comparison

A software implementation of the Matrix Trimetric projection was implemented in Python, using the libraries Numpy (Harris et al., 2020), Scipy (Virtanen et al., 2020), Pandas (Wes McKinney, 2010), GeoPandas (Jordahl et al., 2020), and their dependencies. The implementation of the Chamberlin Trimetric projection comes from PROJ contributors (2019). Because the Chamberlin Trimetric and Matrix Trimetric projections are implemented in different programming languages, one compiled and one interpreted, a comparison of computation time would be unfair and is not included here.

Christensen (1992) gave a list of control triangles for the Chamberlin projection in that paper's Table 1. These serve as a set of test cases for comparing the Chamberlin and Matrix projections. The control triangles are repeated in this text's Table 1. The length of each side and the area of each triangle (with the spherical approximation given earlier) is also given, and the control triangles are sorted by area.

Region	Point			Side length			Area
	1	2	3	1	2	3	
Canada Atlas	98°13'W, 61°39'N	135°W, 40°N	55°W, 40°N	6,560	3,761	3,449	5.28
Canada Wall	150°W, 60°N	97°30'W, 50°N	45°W, 60°N	3,423	5,197	3,423	6.11
NW South America	69°W, 25°S	55°W, 10°N	85°W, 10°N	3,284	4,261	4,177	6.70
Australia	134°E, 8°S	110°E, 32°S	158°E, 32°S	4,487	3,643	3,643	6.76
S South America	43°W, 18°S	72°W, 18°S	72°W, 56°S	4,225	4,874	3,064	6.77
E South America	63°33'W, 8°8'N	58°33'W, 34°35'S	35°13'W, 5°47'S	4,000	3,502	4,779	7.25
Europe Wall	15°E, 72°N	8°W, 33°N	38°E, 33°N	4,254	4,541	4,541	9.09
South America Wall	80°W, 9°N	71°W, 53°S	35°W, 6°S	6,161	5,259	6,947	17.7
North America Wall	150°W, 55°N	92°30'W, 10°N	35°W, 55°N	7,064	6,434	7,064	23.71
Africa Wall	19°3'W, 24°25'N	20°E, 35°S	59°3'E, 24°25'N	7,783	7,785	7,783	32.38

Table 1. Table of control triangles and their measurements. Side n is opposite Point n. Lengths are in km, and areas are in millions of square km.

For each control triangle, some summary statistics for s, ω, and D are calculated. These statistics are measured within the control triangles, and should not be taken to summarize the entire map: for most of the triangles, the region of interest extends outside the control triangle. Rather, the statistics allow a quantitative comparison of the two projections. Some clear trends appear in these figures, Figures 2, 3, and 4. Note that the control triangles are sorted by area in these figures as well, with low area at the bottom and high area at top.

As shown in Figure 2, the Matrix projection consistently has a larger ω than the Chamberlin projection: in fact, the maximum ω for Chamberlin is near the average ω for Matrix. Maximum and average ω trend upwards with control triangle area, although asymmetry of the control triangle has some influence too, as in the Canada triangles. The maximum ω for Matrix is about 3 times that for Chamberlin, and the average ω is about 3 to 4 times. However, for moderately-sized triangles, the maximum ω values are small for both projections, not exceeding 6°. Even for the large triangles – Africa, North America, and South America Wall Maps – the maximum distortion is tolerable, and the average does not exceed 6°.

Distance distortion D in Figure 3 shows an even clearer trend, monotonically increasing with triangle area. Both projections have nearly indistinguishable maximum D values. The Matrix projection has consistently lower average D values than the Chamberlin: among these triangles, the maximum D for Chamberlin is about 1.35 to 1.4 times the maximum D for Matrix. The worst distortion, Africa Wall Map's maximum D, is less than 5% of its edge lengths, and smaller control triangles have a maximum D that is an even smaller percent.

As true 1:1 scale maps are rare, absolute values of s are unimportant: the quantity

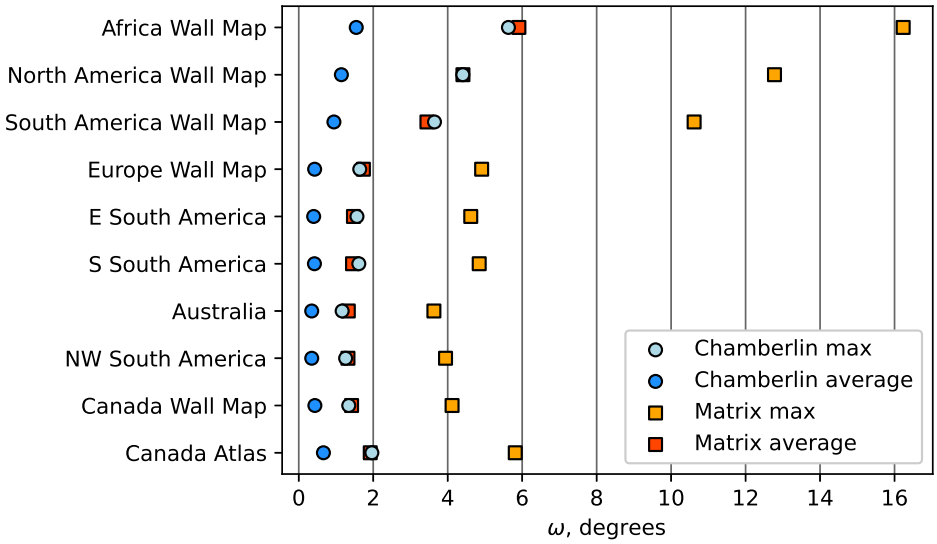

Figure 2. Comparison of angle distortion ω.

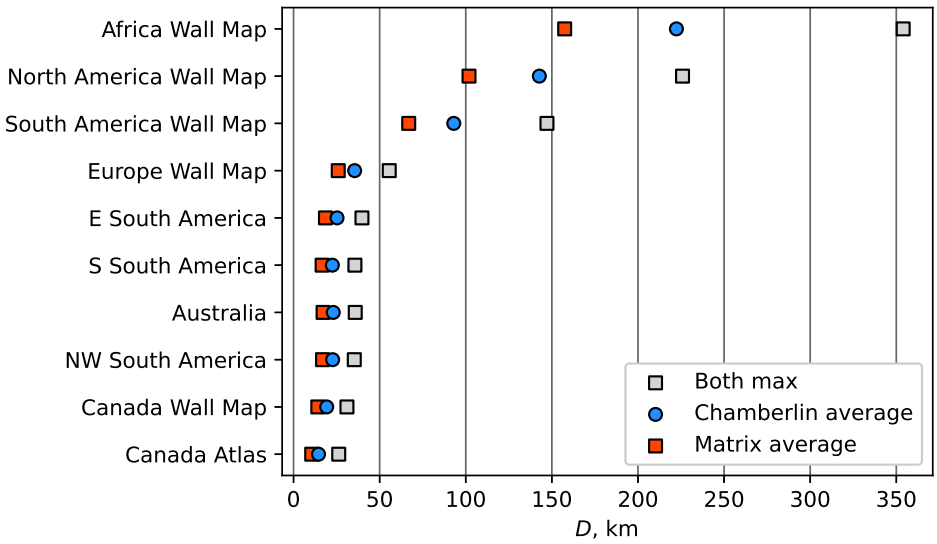

Figure 3. Comparison of total distance distortion D.

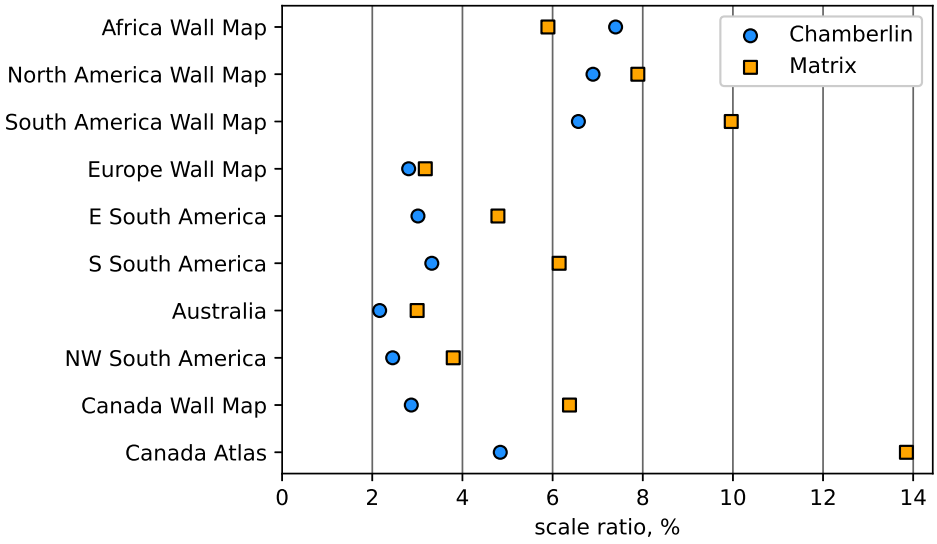

Figure 4. Comparison of area scale distortion $\frac{\max s}{\min s} - 1$.

$\frac{\max s}{\min s} - 1$ is plotted in Figure 4 instead. Scale distortion, $\frac{\max s}{\min s} - 1$, shows a less clear trend. A combination of control triangle area and asymmetry influences this value. In general, this value is higher for Matrix than for Chamberlin, but not by any consistent factor, and for the large and symmetric Africa Wall Map triangle the Matrix projection is lower than Chamberlin. The amount of scale distortion is small for both: except for the very flat Canada Atlas triangle, all values are below 10%.

A comparison of the two projections using the South America Wall Map control points is in Figure 5, using land mass shape files from Patterson and Kelso (2020). The South America Wall Map control triangle is fairly representative, being somewhat asymmetric but not too elongated or compressed. The small part of Central America in the upper left is somewhat shifted between the two maps, as is the western area near Ecuador and Peru, but no features on either map are conspicuously distorted compared to the other. Figure 6 shows ellipses of distortion spaced on a grid at steps of 15° latitude and longitude. Distortion is somewhat more visible in this figure: one can see that the Matrix projection introduces slightly more shearing near the control points.

Contour lines of s are shown in Figure 7. The contour lines have the same circular structure in both projections, centered around a point where s reaches a local minimum. This point is different for each projection, which influences the differences in aggregate area distortion in Figure 4.

Contour lines of ω are shown in Figure 8. Those in the Chamberlin projection have an oval shape, while those for the Matrix Trimetric projection extend outward through each edge of the control triangle. Both reach a minimum ω of 0 at a point inside the control triangle. Highly obtuse control triangles, like Canada Atlas, may have two local minima for ω within the control triangle.

Figure 9 depicts contour lines of D for these two projections. Both projections have a local minimum of 0 at the control points, which follows from the geometric construction. Both have a local maximum near the triangle center. D for the Matrix

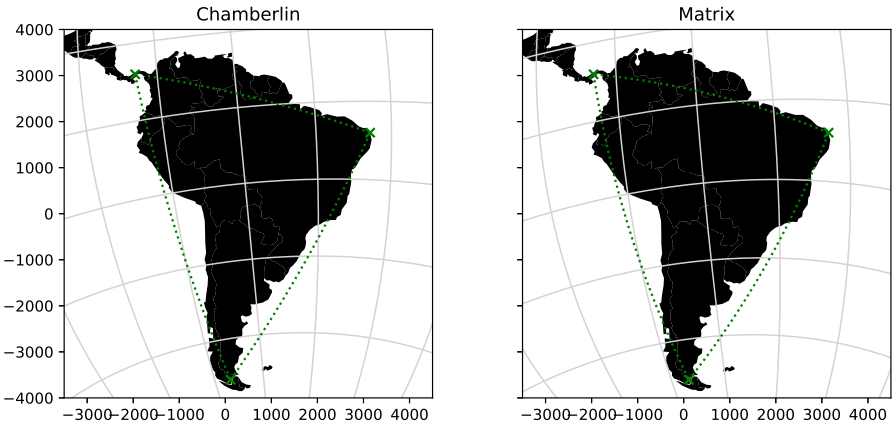

Figure 5. Projection of South America and surroundings.

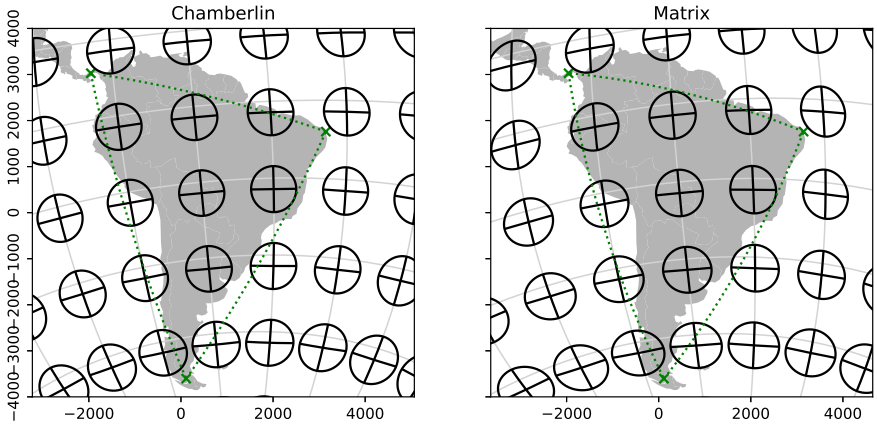

Figure 6. Ellipses of distortion, on a 15 degree grid.

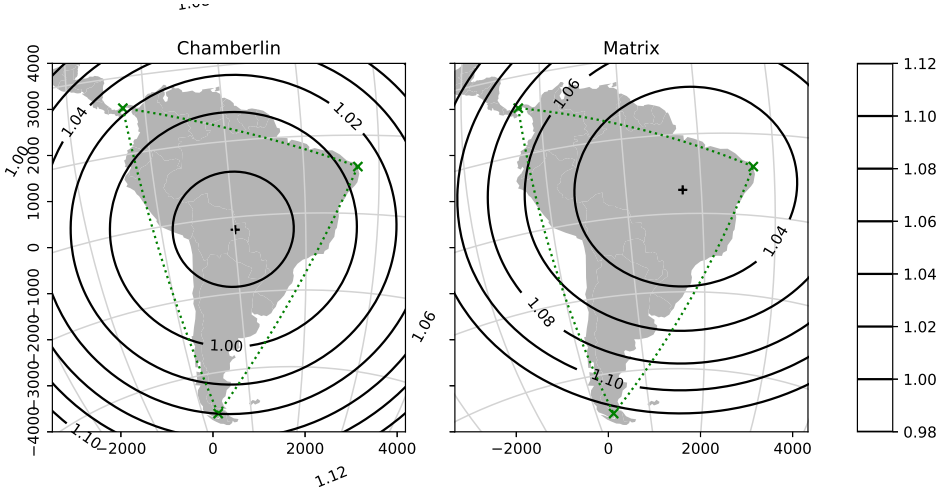

Figure 7. Areal scale factor s.

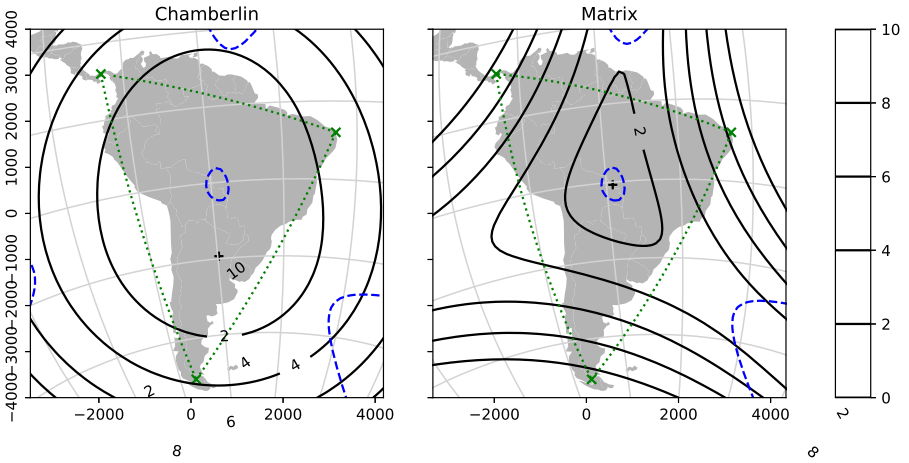

Figure 8. Maximum angular deformation ω, in degrees.

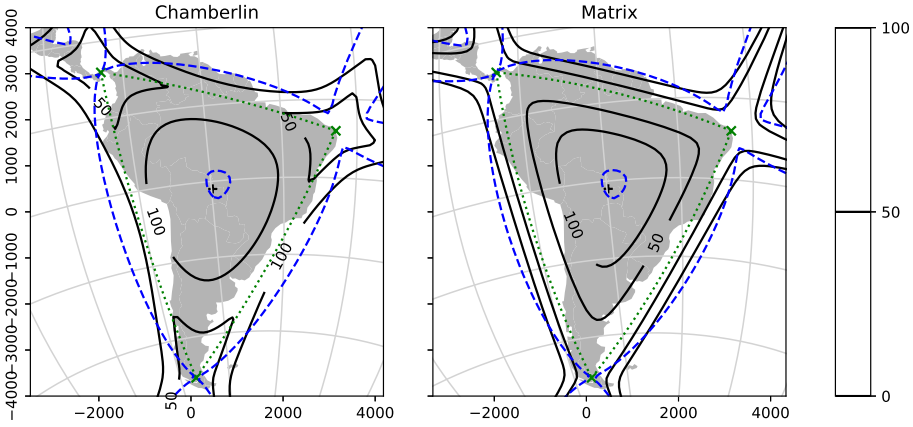

Figure 9. Distance deviation D.

projection is low along the control triangle edges, while for the Chamberlin projection it is larger.

In most practical applications the area pictured in these figures will be sufficient, but it is informative to examine the trend as both projections extend outward from the control triangle. s increases to a maximum and then decreases to 0 at the projection boundary. ω increases to 180 degrees at the projection boundary, representing the inversion of the overlap region. D increases in general, but for the Matrix Trimetric projection D remains low on the great circles containing the control triangle edges.

6. Conclusion

We have demonstrated a new compromise map projection, the Matrix Trimetric projection. The forward formula is given in Equations 6, 7, and 8. Equation 6 is a simple product of a matrix and a vector. The vector depends on the point being transformed. The matrix calculated by the latter two equations depends only on the control points, so can be calculated once and reused for any point on the globe. The forward formula does not have the special cases of the Chamberlin projection, making it more numerically stable as well as more efficient to calculate. Comparisons of calculation time were not made: the Matrix projection would likely be somewhat faster, but for both projections the bulk of calculation time would be spent in the same distance calculations.

The inverse formula is calculated by Equations 9, 10, 12, 11, and a Newton's method iteration using Equations 14 and 15 with the lower bound of Equation 17 as an initial condition. The matrices in Equations 10 and 11 also depend only on the control points, as does matrix $\mathbf{A}$ in Equations 14 and 15, and can be reused. The Chamberlin projection, in contrast, has no known inverse aside from brute force two-variable inversion.

Figures 2, 3, and 4 plot aggregate measures of distortion within each of the listed control triangles. The Chamberlin projection outperforms the Matrix projection in terms of angular distortion and (except in one case) scale distortion, but the reverse is true for distance distortion. For both projections, distortion tends to be larger for a larger control triangle. Figures 5–9 show the projections applied to South America, demonstrating the shape of distortions across the mapped area. Differences between the two projections are small. Apart from the merits of each of these two projections, this shows the value of compromise projections. Projections that eliminate one form of distortion often introduce a great deal of another form of distortion: allowing small amounts of distortion across multiple measures can produce more attractive maps.

The same control points were used for both projections in this work, but the optimal placement of control points may be somewhat different for the application of different projections to the same geographic feature. The angular distortion of the Matrix Trimetric projection is lower in a region extending through the middle of the control triangle edges, so one may wish to orient the triangle to take advantage of that.

The Matrix Trimetric projection is closely related to the Chamberlin projection. Both are related to the azimuthal equidistant projection and the two-point equidistant projection, which depend on measurements from a single point and from a pair of points, respectively.(Snyder, 1987) This suggests an "n-metric" family of projections based on distances from some number of points. The form of the forward formula suggests a possible family of projections that are simple functions of such distances, such as a polynomial function. Additionally, there may exist similar projections using

measurements other than distance, such as area.

The Chamberlin projection implicitly depends on the sphere having nonnegative curvature: otherwise, the circles in the plane would not be guaranteed to intersect. While the derivation presented for the Matrix projection uses the same circles, the formulas are valid for any combination of distances. The Chamberlin projection can be applied to any surface where distances can be defined. For instance, the human brain has concave areas. Brain cortex mapping commonly uses conformal projection, done using iterative algorithms that are often unstable.Angenent, Haker, Tannenbaum, and Kikinis (1999) If the Matrix projection cannot replace conformal projection for this purpose, it may be able to provide it with better initial conditions.

An implementation of the Matrix Trimetric projection, as well as code used to produce the calculations and figures in this text, is available on the author's Github site.(Author, 2020)

References

Angenent, S., Haker, S., Tannenbaum, A., & Kikinis, R. (1999). Conformal geometry and brain flattening. In C. Taylor & A. Colchester (Eds.), *Medical image computing and computer-assisted intervention – miccai'99* (pp. 271–278). Berlin, Heidelberg: Springer Berlin Heidelberg.

Author. (2020). *xxxxxx.* https://github.com/xxxxxxxx/xxxxxxx.

Burden, R., & Faires, J. (2006). Solutions of equations in one variable. In *Numerical analysis* (8.1 ed., pp. 67–85). Cengage Learning.

Christensen, A. H. (1992). The chamberlin trimetric projection. *Cartography and Geographic Information Systems*, *19*(2), 88-100.

Harris, C. R., Millman, K. J., van der Walt, S. J., Gommers, R., Virtanen, P., Cournapeau, D., ... Oliphant, T. E. (2020, September). Array programming with NumPy. *Nature*, *585*(7825), 357–362. Retrieved from `https://doi.org/10.1038/s41586-020-2649-2`

Jordahl, K., den Bossche, J. V., Fleischmann, M., Wasserman, J., McBride, J., Gerard, J., ... Leblanc, F. (2020). *geopandas/geopandas: v0.8.1.* https://zenodo.org/record/3946761. Zenodo. Retrieved from `https://zenodo.org/record/3946761`

Patterson, T., & Kelso, N. V. (2020). *Natural earth.* https://www.naturalearthdata.com/. (Accessed: 2020-01-17)

Posamentier, A., & Salkind, C. (2012). *Challenging problems in geometry.* Dover Publications.

PROJ contributors. (2019). PROJ coordinate transformation software library [Computer software manual]. Retrieved from `https://proj.org/`

Snyder, J. P. (1987). *Map projections–a working manual* (No. 1395). US Government Printing Office.

Snyder, J. P., & Voxland, P. M. (1989). *An album of map projections* (No. 1453). US Government Printing Office.

Strang, G. (1980). *Linear algebra and its applications.* Academic Press.

Virtanen, P., Gommers, R., Oliphant, T. E., Haberland, M., Reddy, T., Cournapeau, D., ... SciPy 1.0 Contributors (2020). SciPy 1.0: Fundamental Algorithms for Scientific Computing in Python. *Nature Methods*, *17*, 261–272.

Wes McKinney. (2010). Data Structures for Statistical Computing in Python. In Stéfan van der Walt & Jarrod Millman (Eds.), *Proceedings of the 9th Python in*

Science Conference (p. 56 - 61).
Wohlgemuth, M. (2010). *Mathematisch für fortgeschrittene anfänger: Weitere beliebte beiträge von matroids matheplanet.* Spektrum Akademischer Verlag.